PHYSICAL REVIEW B **71**, 045417 (2005)

Photoexcited electron relaxation processes in single-wall carbon nanotubes

J. Jiang,[1] R. Saito,[1] A. Grüneis,[1] S. G. Chou,[2] Ge. G. Samsonidze,[3] A. Jorio,[4,5] G. Dresselhaus,[6] and M. S. Dresselhaus[3,4]
[1]*Department of Physics, Tohoku University and CREST, JST, Sendai, 980-8578, Japan*
[2]*Department of Chemistry, Massachusetts Institute of Technology, Cambridge, Massachusetts 02139-4307, USA*
[3]*Department of Electrical Engineering and Computer Science, Massachusetts Institute of Technology, Cambridge, Massachusetts 02139-4307, USA*
[4]*Department of Physics, Massachusetts Institute of Technology, Cambridge, Massachusetts 02139-4307, USA*
[5]*Departamento de Física, Universidade Federal de Minas Gerais, Belo Horizonte—MG, 30123-970 Brazil*
[6]*Francis Bitter Magnet Laboratory, Massachusetts Institute of Technology, Cambridge, Massachusetts 02139-4307, USA*
(Received 2 August 2004; revised manuscript received 11 October 2004; published 14 January 2005)

The relaxation processes for photoexcited electrons in single-wall carbon nanotubes (SWNTs) are discussed in connection with recent photoluminescence excitation (PLE) spectroscopy experiments. The electron-phonon (*e*-ph) interaction of SWNTs is calculated for each phonon mode as a function of photoexcited electron energy. Because of the cylindrical surface of a SWNT, the twisting and radial breathing phonon modes are responsible for the *e*-ph interaction in the lower phonon energy region. Optic phonon modes are also responsible for the relaxation of photoexcited electrons. Compared with graphite, the relaxation of electrons is much faster in SWNTs because of their cylindrical shape. We identify and explain some aspects of both photoluminescent and Raman processes appearing in PLE plots for SWNTs.

DOI: 10.1103/PhysRevB.71.045417 PACS number(s): 78.67.−n, 78.40.−q, 78.30.−j

I. INTRODUCTION

Isolated semiconducting single-wall carbon nanotubes (SWNTs) show fluorescence (FL) or photoluminescence (PL) at the energy gap[1,2] known as E_{11}, whose energy depends on the chirality (n,m) of the SWNT.[3] Bachilo *et al.* plot the PL intensity as a function of the excitation and the emission wavelength (or energy) in which many bright spots can be assigned to specific (n,m) values for individual SWNTs.[4] We refer to this plot hereafter as the two-dimensional photoluminescence excitation plot (or simply the PLE plot). Each spot on the PLE plot corresponds to the photo absorption at E_{22} and the photo emission at E_{11}, which is known as the Stokes shift of PL. A photoexcited electron is relaxed by phonon emission (1) from an energy subband for E_{22} to that for E_{11} (interband transition, EB), and then (2) the electron is relaxed within the subband of E_{11} to the bottom of the conduction band at E_{11} (intraband transition, AB).[5–8] A similar relaxation process occurs for a photoexcited hole in the valence band. In the case of hole relaxation, we also need the emission of phonons.

For the electronic energy bands of a semiconducting SWNT, we know that the energy subbands are twofold degenerate, which originates from the one-dimensional (1D) Brillouin zone (BZ) of a SWNT (or a cutting line[9]) near the K and K' points in the graphite two-dimensional (2D) BZ.[3] Thus the emitted phonon consists of either intravalley (AV) or intervalley (EV) scattering for $\{(K \text{ to } K), (K' \text{ to } K')\}$ $\{(K \text{ to } K'), (K' \text{ to } K)\}$, respectively, which correspond to phonons near the Γ and K points of the 2D BZ of graphite.[10]

Thus we will consider four different electron-phonon scattering processes: ABAV, ABEV, EBAV, EBEV (Fig. 1). Strictly speaking, ABEV scattering is not an intraband scattering process, since the two energy subbands are separated from each other in the k space of 2D graphite. However, we hereafter call them "AB" for simplicity.

Generally, the recombination of an electron and a hole by emitting a *photon* has a much slower speed (1 ns) than the relaxation by emitting a *phonon* (0.1 ps) in most direct gap semiconductors.[11] Thus we can expect the band-gap PL to occur at the energy minimum after many phonon emission processes. However, we expect PL also to occur before going to the E_{11} energy and this process is called *hot electron luminescence*. This process may occur when the lower-energy states in the conduction band are occupied by photoexcited electrons. In our previous paper,[12] we discussed the relaxation of excited electrons in graphite, in which the emission and absorption relaxation rates become almost the same at a certain energy at which the electron-hole pairs recombine with each other. The reason why we get the same relaxation rate for the emission and absorption processes is due to the fact that the density of states (DOS) of graphite decreases to zero with decreasing electron energy in the conduction band (sand clock effect).[12] This is the reason why graphite emits far infrared light in spite of the absence of an energy gap at the Fermi level.

Moreover, we have a Raman process that occurs independently and involves a virtual state in the photon emission process. Thus many kinds of spectra should be seen in the PLE plot associated with the many different photo-excited relaxation processes.[13] In this theoretical work, we consider the possible relaxation processes in semiconducting SWNTs by calculating electron-phonon matrix elements.

In Sec. II we first enumerate the possible photoprocesses and show how we can see each of them in the PLE plot. In Sec. III we quantitatively evaluate the relaxation time of a photoexcited electron for each phonon mode as a function of the electron energy relative to E_{11}, and we try to understand what is happening in the PL process and in fast optics experiments. In Secs. IV and V a discussion and summary are given.

©2005 The American Physical Society

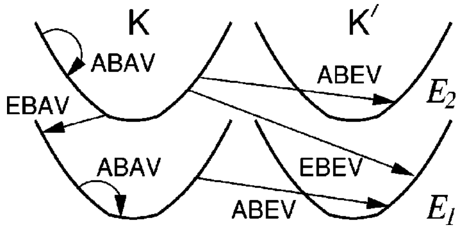

FIG. 1. Four different kinds of photoexcited electron relaxation processes which connect the two conduction bands (E_1 and E_2) at the K and K' points of the two-dimensional Brillouin zone. ABAV (intraband, intravalley), EBAV (interband, intravalley), ABEV (intraband intervalley), EBEV (interband, intervalley) scattering processes.

II. CLASSIFICATION OF THE RELAXATION PROCESSES

First we discuss the relaxation processes within an (n,m) semiconductor SWNT and neglect relaxation processes to the other nanotubes. As discussed in the Introduction, many possible processes for different kinds of phonons are involved in electron-phonon scattering processes. Most of the PL signal is observed at the energy E_{11} in which both electrons and holes are relaxed to the conduction band minimum and the valence band maximum, respectively, before recombination. Since the joint density of states (JDOS) at E_{ii} is singular (known as a van Hove singularity, vHS), the PL at E_{11} has the strongest intensity. When we see this luminescence in an experimental PLE plot (the excitation energy E_{ex} as a function of the PL energy E_{PL}), the PL intensity appears along the vertical line of $E_{\mathrm{PL}}=$const and E_{ex} can have any value satisfying $E_{\mathrm{ex}} \geqslant E_{11}$.

If an electron is relaxed from an energy state at k of the energy dispersion relation $E(i,k)$ to $E(j,k+q)$ by emitting a phonon with wave vector q of the νth phonon branch $\hbar\omega^{\nu}(\mu,q)$, the energy momentum conservation should satisfy

$$E(i,k) - E(j,k+q) = \hbar\omega^{\nu}(\mu,q). \tag{1}$$

The intraband and interband transitions (AB and EB) correspond to $i=j$ and $i\neq j$, respectively, while the intravalley and intervalley transitions (AV and EV), respectively, correspond to zone center ($q\sim 0$) and zone boundary ($q\sim \Gamma K$) phonon modes.[10]

The wave vectors k in Eq. (1) are defined by 1D wave vectors. In the zone-folding scheme from 2D graphite, the 2D wave vector $\mathbf{k}$ can be expressed by $\mathbf{k}=\mu\mathbf{K}_1+k\mathbf{K}_2$, where $\mu=1,\ldots,N$, and $-\pi/T<k<\pi/T$, thereby defining μ in Eq. (1).[3] Here $\mathbf{K}_1$ and $\mathbf{K}_2$ are, respectively, the reciprocal lattice vectors along the circumferential and axial directions, and T and N are, respectively, the 1D translational vector and the number of hexagons in the 1D nanotube unit cell.[3] Because of energy-momentum conservation of the electron and the phonon, the emitted phonon has the subband index $\mu=j-i$.[3,9] In the case of AV phonon emission, the symmetries of the phonons are A ($\mu=0$) and E_1 ($\mu=\pm 1$), respectively, for ABAV and EBAV scattering.[3] For EV phonon emission, the μ values depend on (n,m) and more specifically on the particular $2n+m=$constant family of each SWNT. Here the S1 and S2 families of SWNTs are defined by mod$(2n+m,3)$ $=1$, and 2, respectively.[14] For small diameter SWNTs, the E_{11} energy appears on a curve for each $2n+m=$constant family in the PLE experiment.[15]

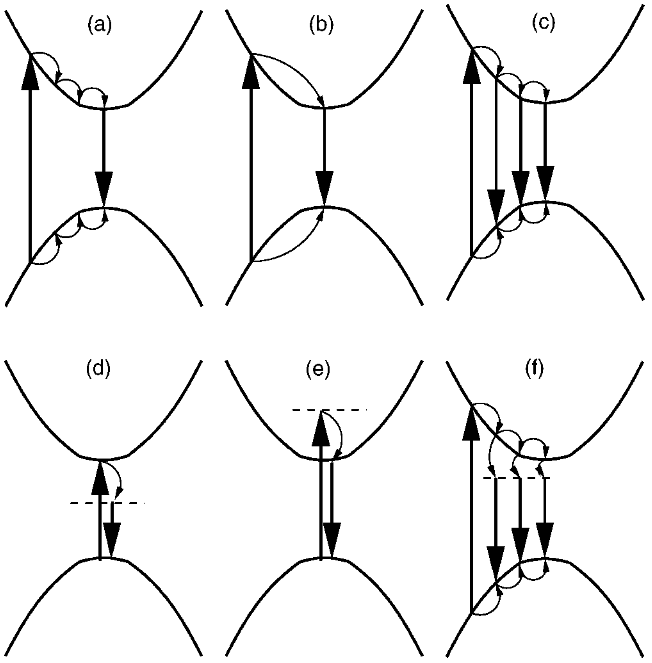

FIG. 2. Possible ABAV processes. (a) PL, (b) two-phonon emission, (c) hot-electron emission, (d) incident resonance one-phonon Raman process, (e) scattered one-phonon Raman process, (f) hot-electron Raman process.

After some calculation, we get the following formulas for the μ values for EV phonons for transitions from energy bands E_i to E_j (see Fig. 2), which are listed in Table I. It is noted that the μ values in Table I are for normal scattering processes in which the electron is scattered within the 1D BZ. When T is large, the length of the 1D BZ becomes short, and thus Umklapp scattering can be expected. In Table I, we did not consider these Umklapp scattering processes. In the numerical calculations, we have considered all possible phonon energy subbands for momentum-energy conserved **q** vectors, including umklapp processes. As we can imagine, the numbers of energy-momentum conserved **q** vectors are generally 12 for AV and 12 for EV, which correspond to the 6 phonon modes in 2D graphite. If no phonon energy exists for a certain **q** value, there are no energy-momentum conserved **q** vectors. Among the 12 **q** vectors, 6 **q** vectors exist

TABLE I. The μ values for intervalley (EV) phonon scattering for S1 and S2 semiconducting SWNTs. Note that the μ value for $E_2\to E_1$ for EBEV is the same as that for $E_1\to E_2$ (see Fig. 1 for definition of E_1, E_2).

Transition	Symbol	S1	S2
$E_1\to E_1$	ABEV	$(2n+m-1)(2/3)$	$(2n+m+1)(2/3)$
$E_2\to E_2$	ABEV	$(2n+m+2)(2/3)$	$(2n+m-2)(2/3)$
$E_1\to E_2$	EBEV	$(4n+2m+1)(1/3)$	$(4n+2m-1)(1/3)$

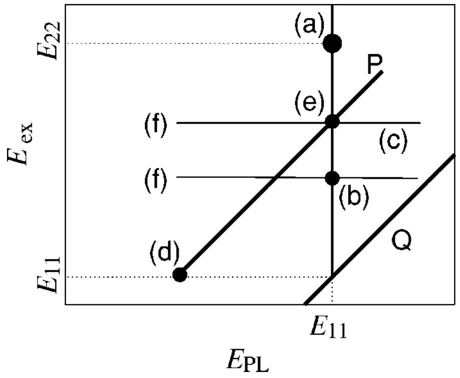

FIG. 3. Schematic view of PLE diagram; (a) to (f) correspond to the processes of Fig. 2. Lines P and Q are Raman and Rayleigh processes, respectively.

on the same side relative to the van Hove singular q point in the phonon energy dispersion, and the other 6 $\mathbf{q}$ vectors exist on the other side of the vHS q point. In the ABAV process, there are two zero frequency, energy-momentum conserved phonon modes, and thus the number of $\mathbf{q}$ vectors is reduced to 10.

In Fig. 2, we illustrate the possible ABAV scattering processes. We show the relaxation processes only for the same side of the vHSs relative to the energy minimum for simplicity. The processes from (a) to (c) correspond to PL processes and from (d) to (f) correspond to Raman processes in which we expect virtual states denoted by dashed lines. Figure 2(a) represents the normal PL process occurring at the energy E_{11} in which both an electron and a hole relax to their respective energy extrema by emitting many phonons. In the schematic PLE plot [see Fig. 3(a)], a bright spot can be observed in the experiment at $(E_{\mathrm{PL}},E_{\mathrm{ex}})=(E_{11},E_{22})$ for the normal PL process.

Before completing the normal PL process in Fig. 2(a), some electrons will be lost before arriving at E_{11} by a hot-emission process [see Fig. 2(c)]. Then the condition to have a bright spot for the normal PL process is that electrons are excited to a vHS, e.g., E_{22}, to enhance the optical absorption intensity. When the laser energy is smaller than E_{22}, we can still see PL at E_{11}, but now by the process in Fig. 2(b), shown by the vertical line in Fig. 3.

Figure 2(b) corresponds to a special case where the initial state has the same energy as a phonon energy above E_{11}. In this case, an electron and hole can each jump to their respective energy extrema directly by emitting this special phonon and thus we can expect a peak at $(E_{\mathrm{PL}},E_{\mathrm{ex}})=(E_{11},E_{11}+2\hbar\omega)$ [see (b) point of Fig. 3]. Here we use the fact that the conduction and valence energy bands are almost symmetric relative to the Fermi energy so that the same phonon mode is involved for both electrons and holes in process (b). The reason why we expect a peak at this energy at point (b) is that the energy-momentum condition for this phonon mode will not be satisfied for an energy below or above this energy at point (b). An easy example for understanding this in normal life is the fact that the traveling time to a destination is small (fast process) only from the express-train stopping stations. Hereafter, we call the process in Fig. 2(b) a *two-phonon emission* process where $E_{\mathrm{ex}}=E_{11}+2\hbar\omega$.

Figure 2(c) represents a hot-electron luminescence process. When an electron and hole pair has the same k vector for an instant of time, there is a probability for the electron and hole to recombine at a higher energy point than E_{11}. This can be seen by the horizontal line in Fig. 3 and for $E_{\mathrm{PL}}>E_{11}$. In general, there is no restriction on E_{ex} for observing a hot-electron process. However, when process (b) can occur, then process (c) may become strong, since there are then many electron-hole pairs waiting to recombine in a luminescence process (we showed that the photon relaxation time is much longer than the phonon relaxation time). Thus slow electrons and holes cannot go to the energy extrema because of the Pauli exclusion principle and then a hot-electron luminescence process is expected. Thus it would be interesting to observe PL experiments by illuminating the sample with photons of energy E_{11} in which we would expect a strong hot luminescence signal.

From (d) to (f) in Fig. 2, we show Raman processes observed in the PL experiment. Figure 2(d) shows the incident resonance conditions $(E_{\mathrm{PL}},E_{\mathrm{ex}})=(E_{11}-\hbar\omega,E_{11})$, which gives a bright spot at (d) in Fig. 3. For a general E_{ex}, a strict resonance condition, gives a PLE signal at the points $(E_{\mathrm{PL}},E_{\mathrm{ex}})=(E_{\mathrm{ex}}-\hbar\omega,E_{\mathrm{ex}})$ for $E_{11}<E_{\mathrm{ex}}<E_{11}+\hbar\omega$ which gives a line with a 45° slope, as shown by P in Fig. 3. Another 45° slope Q in Fig. 3 is Rayleigh scattering $(E_{\mathrm{ex}}=E_{\mathrm{PL}})$. For a higher energy of E_{ex} than E_{11}, the scattered resonance condition [Fig. 2(e)] can be expected and the corresponding PLE spot is $(E_{\mathrm{PL}},E_{\mathrm{ex}})=(E_{11},E_{11}+\hbar\omega)$ [(e) in Fig. 3] and the 45° line at $(E_{\mathrm{PL}},E_{\mathrm{ex}})=(E_{\mathrm{ex}}-\hbar\omega,E_{\mathrm{ex}})$ for $E_{\mathrm{ex}}>E_{11}+\hbar\omega$ is shown by P in Fig. 3. The combination of a hot-electron and Raman process is shown in Fig. 2(f). This process gives a horizontal line in the PLE plot at an energy $E_{11}-\hbar\omega<E_{\mathrm{PL}}$, as shown in Fig. 3(f). Again this horizontal line might be seen only for a special E_{ex} which corresponds to the (b) or (e) processes of Fig. 2 in which we also expect a peak on the vertical line of $E_{\mathrm{PL}}=E_{11}$.

A recent PLE experiment for a (6,5) enriched DNA-wrapped SWNT sample[16] exhibits the peaks and the lines shown in Fig. 3 in the schematic PLE plot.[17] By using the calculated phonon frequencies, we can predict the energy positions by analyzing the relaxation routes for the ABAV, EBAV, ABEV, and EBEV processes. Moreover, a double resonance Raman condition can be expected in which two phonons are involved in the Raman process.[10]

So far we do not consider relaxation from or to another SWNT. If the sample is enriched with a single (n,m) SWNT, the spectra would not be changed. However, when we have a relatively large diameter SWNT near a given SWNT of smaller diameter, we can expect a relaxation process to occur for the larger diameter SWNT, since the larger SWNT has a smaller E_{11}' value [see Fig. 4(a)]. As a result, we will see two vertical lines at E_{11} and E_{11}', respectively [Fig. 4(b)]. The bright spots due to the *two-phonon emission* process are indicated on the vertical line at the larger E_{11} in Fig. 4(b). A series of bright spots due to *one-phonon emission* process also exist on the vertical line at the smaller E_{11}' and are not shown in Fig. 4(b). The spots on the vertical line at a smaller E_{11}' value may be brighter since some electrons will relax

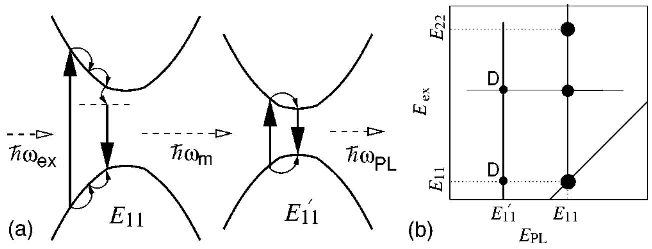

FIG. 4. (a) Internanotube transition from a smaller diameter SWNT with a larger E_{11} to a SWNT with a smaller E'_{11}. (b) On the vertical line at $E_{PL}=E'_{11}$ some "dummy spots" D are observed which do not originate from a phonon mode of the smaller E'_{11} SWNT.

from the larger E_{11} SWNT to the smaller E'_{11} SWNT. When a horizontal line generated by the large E_{11} SWNT crosses the smaller E'_{11} SWNT vertical line in the PLE plot, we expect a small peak D at the crossing point, which corresponds to the relaxation to the smaller E'_{11} SWNT, even though the E_{ex} does not correspond to either the (b), (c), or (e) processes of Fig. 2 for the smaller E'_{11} SWNT. Thus when we measure the PLE spectra for a mixed semiconductor SWNT sample, we must be careful for such "dummy peaks" which occur by optical excitation of one (n,m) SWNT and photon emission by another (n',m') SWNT of larger diameter d_t and therefore smaller E'_{11} value. The interaction between two SWNTs can be mediated either by photon radiation or by an electron tunneling process. It should be very interesting to control these processes between two SWNTs in the experiments.

When we have a semiconducting SWNT near a metallic SWNT, e.g., in a multiwall nanotube (MWNT) or a bundle of SWNTs with at least one shell of metallic nanotube, we can expect electrons and holes at the energy extrema of the semiconducting nanotube to tunnel to the metallic bands of the metallic nanotube. The electrons and holes at the metallic bands then relax to the Fermi level to combine without PL emission. There is almost no hot-electron emission in the process of electrons and holes for metallic bands relaxing to the Fermi level due to the nodes of the optical transition matrix for the metallic bands.[18] We can estimate the tunneling rate of electrons between walls of a multiwall nanotubes by $1/\tau=(2\pi/\hbar)|H'|^2\rho$, where τ is the relaxation time, H' the electron interaction between two walls, and ρ the density of states for electronic energy bands of a metallic nanotube. By considering that the π electron hopping integral along the c axis of graphite is about 0.35 eV,[19,20] we can take $|H'|\approx 0.35$ eV. The density of states per carbon per spin can be estimated by $\rho\approx\rho(\epsilon_F)=a/(\pi^2|t|d_t)$ with the transfer integral $|t|\approx 2.9$ eV. It follows that $\tau\approx(8.4\times10^{-3}|t|d_t)/a$ ps. For a metallic shell with a diameter about 1 nm, the tunneling speed is on the order of 0.1 ps. From the following discussions we can see that the phonon relaxation rate in SWNTs can reach 0.01 ps. Thus the electron tunneling speed is slower than the phonon emission speed but much faster than the photon emission speed. As a result, we expect that the bright spots on the vertical line at energy E_{11} of the semiconducting nanotube will disappear, while the horizontal lines (see Fig. 3) will still exist. Therefore, MWNTs with metallic shells provide a good material to observe hot-electron luminescence processes directly.

It seems that a double resonance process for overtone phonon modes cannot be distinguished from process (b) in Fig. 2, from an energy point of view, since both processes reduce the electron energy by $2\hbar\omega$. However, these two processes are different from each other as to whether or not there are virtual states. In fact, we expect a spot (b) in Fig. 3 for the *two-phonon emission* process of Fig. 2 on the vertical line at $E_{PL}=E_{11}$, while we expect for a double resonance overtone process corresponding to a line with nearly 45° in Fig. 3, for which, the energy condition $E_{ex}=E_{PL}+\hbar(\omega_1+\omega_2)$ will be satisfied. The departure from 45° reflects the dispersive character of the double resonance Raman process, e.g., G' band, as the excitation energy is varied.

In order to know the relative intensity of the PLE peaks, we need to do quantitative calculations of the pertinent electron-phonon interactions. The electron-phonon interactions were studied, focusing on the conductivity and low-energy electronic structure of SWNTs.[21,22] So far we have developed a program to calculate electron-phonon interactions and we have applied this calculation to graphite.[12,23] In the following, we show how to modify the program so that it is suitable for a SWNT. In the next section, we show the formula for the electron-phonon matrix elements and some calculated results that explain the experimental results observed for the PLE plots for a (6,5) SWNT.[17]

III. ELECTRON-PHONON MATRIX ELEMENT AND RELAXATION TIME

A periodic displacement of atoms around the equilibrium sites gives rise to electron-phonon interaction that can be treated in first-order time-dependent perturbation theory. The electron-phonon matrix element D thus obtained is given below in Eq. (10). In order to estimate D, we need to know the electron wave function coefficient C_s, which is obtained by diagonalizing a 2×2 Hamiltonian matrix. The phonon eigenvector $\mathbf{e}(\mathbf{q})$ in Eq. (10) described below is obtained by diagonalizing N 6×6 dynamical matrices. The atomic deformation potential vector $\mathbf{m}$ is a three-center integral and we evaluate this integral by fitting the carbon $2p_z$ orbital and carbon atomic potential by a set of Gaussians. With the help of the matrix element D, the electron scattering probability by phonons is calculated by the Fermi golden rule and the result is given in Eq. (15) from which the relaxation time can readily be estimated.

A. Deformation potential vector

The dynamical matrix for phonon dispersion relations in a SWNTs is a $6N\times6N$ matrix.[3] However, due to the C_N symmetry,[3] the phonon eigenvector for the j^{th} A (or B) atom can be expressed by

$$\mathbf{e}^{\nu}_{j\sigma}(\mathbf{q}) = e^{i\mathbf{q}\cdot\mathbf{R}_{j\ell}}U^{(j-\ell)}\mathbf{e}^{\nu}_{\ell\sigma}(\mathbf{q}), \tag{2}$$

where $\sigma=A,B$, and $\mathbf{R}_{j\ell}$ is the coordinate of the j^{th} A (or B) atom measured from the ℓth A (or B) atom and U is a rotation matrix around the z axis. With the help of Eq. (2), the $6N\times6N$ dynamical matrix is decoupled to become N 6×6

matrices. We can then work within the graphite unit cell, which has only one (A,B) atom pair.

We can write an expression for the interaction Hamiltonian for the electron-phonon coupling in the form[12]

$$H_{e\text{-ph}} = \langle \Psi(\mathbf{r},\mathbf{k}',t) | \delta V(\mathbf{r},t) | \Psi(\mathbf{r},\mathbf{k},t) \rangle, \tag{3}$$

where $\Psi(\mathbf{r},\mathbf{k},t)$ and $\Psi(\mathbf{r},\mathbf{k}',t)$ are the initial and final electron states, respectively, and $\delta V(\mathbf{r},t)$ is the deformation potential. Here we focus on the electron-phonon interaction for electrons in the conduction band. The wave function $\Psi(\mathbf{r},\mathbf{k},t)$ for conduction band electron states in SWNTs is given by

$$\Psi(\mathbf{r},\mathbf{k},t) = \frac{1}{\sqrt{N_u}} \sum_{s=A,B} \sum_{\mathbf{R}_s}^{N_u} C_s(\mathbf{k}) e^{i[\mathbf{k}\cdot\mathbf{R}_s - \omega(\mathbf{k})t]} \phi(\mathbf{r}-\mathbf{R}_s), \tag{4}$$

where $\omega(\mathbf{k}) = E(\mathbf{k})/\hbar$, $\phi(\mathbf{r}-\mathbf{R}_s)$ is the $2p_z$ orbital of carbon, and N_u is the number of graphite unit cells in the SWNT. The coefficient $C_s(\mathbf{k})$ and energy $E(\mathbf{k})$ are obtained by diagonalizing the 2×2 Hamiltonian matrix.[3] The deformation potential $\delta V(\mathbf{r},t)$, including all atoms in the SWNT, is given by

$$\delta V(\mathbf{r},t) = -\sum_{\sigma=A,B} \sum_{\mathbf{R}_\sigma}^{N_u} \mathbf{u}(\mathbf{R}_\sigma,\mathbf{q}) \cdot \nabla v(\mathbf{r}-\mathbf{R}_\sigma), \tag{5}$$

where $\mathbf{u}(\mathbf{R}_\sigma,\mathbf{q})$ is the atomic displacement and $v(\mathbf{r}-\mathbf{R}_\sigma)$ is the atomic potential at the $\mathbf{R}_\sigma$ site. In terms of the phonon eigenvector $\mathbf{e}_\sigma^\nu(\mathbf{q})$, we get an expression for the atomic displacement

$$\mathbf{u}(\mathbf{R}_\sigma,\mathbf{q}) = \frac{1}{2} \sum_{\mathbf{q},\nu} A_\nu(\mathbf{q}) \mathrm{Re}\left[e^{i\{\mathbf{q}\cdot\mathbf{R}_\sigma - \omega_\nu(\mathbf{q})t\}} U(\mathbf{R}_\sigma) \mathbf{e}_\sigma^\nu(\mathbf{q})\right], \tag{6}$$

where $A_\nu(\mathbf{q})$ is the atomic vibration amplitude, $\omega_\nu(\mathbf{q})$ is the phonon eigenvalue, and $\mathrm{Re}[\cdots]$ denotes the real part of a complex function. The atomic vibration amplitude $A_\nu(\mathbf{q})$ is expressed by

$$A_\nu(\mathbf{q}) = \left[\frac{\hbar}{N_u M \omega_\nu(\mathbf{q})}\right]^{1/2}, \tag{7}$$

where M is the carbon atom mass. By considering the relationship,

$$\begin{aligned} &\langle \Psi(\mathbf{r},\mathbf{k}',t) | \nabla v(\mathbf{r}-\mathbf{R}'_\sigma) | \Psi(\mathbf{r},\mathbf{k},t) \rangle \\ &\quad = e^{i(\mathbf{R}'_\sigma - \mathbf{R}_\sigma)\cdot(\mathbf{k}-\mathbf{k}')} U(\mathbf{R}'_\sigma - \mathbf{R}_\sigma) \\ &\qquad \times \langle \Psi(\mathbf{r},\mathbf{k}',t) | \nabla v(\mathbf{r}-\mathbf{R}_\sigma) | \Psi(\mathbf{r},\mathbf{k},t) \rangle, \end{aligned} \tag{8}$$

the e-ph Hamiltonian can finally be expressed as

$$\begin{aligned} H_{e\text{-ph}} = &-\frac{1}{2} \sum_{\mathbf{k},\mathbf{k}'} \sum_{\mathbf{q},\nu} A_\nu(\mathbf{q}) D_\nu(\mathbf{k},\mathbf{k}') \\ &\times \left[e^{-i[\omega(\mathbf{k}')-\omega(\mathbf{k})-\omega_\nu(\mathbf{q})]t} + e^{-i[\omega(\mathbf{k}')-\omega(\mathbf{k})+\omega_\nu(\mathbf{q})]t}\right] \delta_{\mathbf{k}',\mathbf{k}+\mathbf{q}}. \end{aligned} \tag{9}$$

Here we have introduced a matrix element $D_\nu(\mathbf{k},\mathbf{k}')$,

$$\begin{aligned} D_\nu(\mathbf{k},\mathbf{k}') = &\sum_{s,s',\sigma=A,B} \sum_{\mathbf{R}'_s,\mathbf{R}_s}^{N_u} C_{s'}^*(\mathbf{k}') C_s(\mathbf{k}) \mathbf{m}_\sigma(\mathbf{R}_{s'},\mathbf{R}_s) \cdot \mathbf{e}_\sigma^\nu(\mathbf{q}) \\ &\times e^{-i\mathbf{k}'\cdot(\mathbf{R}_{s'}-\mathbf{r}_\sigma)} e^{i\mathbf{k}\cdot(\mathbf{R}_s-\mathbf{r}_\sigma)}, \end{aligned} \tag{10}$$

in which $\mathbf{r}_\sigma$ is the atomic potential site for a given graphite unit cell, and $\mathbf{m}$ in Eq. (10) is the atomic deformation potential vector,

$$\mathbf{m}_\sigma(\mathbf{R}_{s'},\mathbf{R}_s) = \int \phi(\mathbf{r}-\mathbf{R}_{s'}) \nabla v(\mathbf{r}-\mathbf{r}_\sigma) \phi(\mathbf{r}-\mathbf{R}_s) d\mathbf{r}, \tag{11}$$

and $M_\nu(\mathbf{k},\mathbf{k}') = A_\nu(\mathbf{q}) D_\nu(\mathbf{k},\mathbf{k}')$ gives the e-ph matrix element. The scattering probability from an initial $\mathbf{k}$ state to a final $\mathbf{k}'$ state is given by the Fermi golden rule,

$$\begin{aligned} W_{\mathbf{k}\to\mathbf{k}'}^\nu = &\frac{\pi}{2N_u M \omega_\nu(\mathbf{q})} |D_\nu(\mathbf{k},\mathbf{k}')|^2 (1-n_{\mathbf{k}'}) n_{\mathbf{k}} \\ &\times \{n_{\mathbf{q},\nu} \delta(E(\mathbf{k}') - E(\mathbf{k}) - \hbar\omega_\nu(\mathbf{q})) + (n_{\mathbf{q},\nu} \\ &+ 1) \delta(E(\mathbf{k}') - E(\mathbf{k}) + \hbar\omega_\nu(\mathbf{q}))\} \delta_{\mathbf{k}',\mathbf{k}+\mathbf{q}}. \end{aligned} \tag{12}$$

The first and second terms in Eq. (12) correspond to the absorption and emission probabilities, respectively, and the two δ functions provide for energy and quasimomentum conservation. For the optical excitation of an electron, we can set $n_{\mathbf{k}} = 1$ and $n_{\mathbf{k}'} = 0$, while $n^\nu(\mathbf{q})$ is determined by the Bose-Einstein distribution function. For phonon emission, $n_{\mathbf{q},\nu}$ is given by

$$n_{\mathbf{q},\nu} = \frac{1}{e^{\beta\hbar\omega} - 1} + 1, \tag{13}$$

and for phonon absorption we have

$$n_{\mathbf{q},\nu} = \frac{1}{e^{\beta\hbar\omega} - 1}. \tag{14}$$

Here $\beta = 1/k_{\mathrm{B}}T$ and k_{B} is the Boltzmann constant. The scattering probability $W_{\mathbf{k}}^\nu$ from an initial state $\mathbf{k}$ to all possible final states $\mathbf{k}'$ is given by

$$\begin{aligned} W_{\mathbf{k}}^\nu = &\frac{S}{8\pi M d_t} \sum_{\mu',k'} \frac{|D_\nu(\mathbf{k},\mathbf{k}')|^2}{\omega_\nu(\mathbf{k}'-\mathbf{k})} \left[\frac{dE(\mu',k')}{dk'}\right]^{-1} \\ &\times \left\{ \frac{\delta(\omega(\mathbf{k}') - \omega(\mathbf{k}) - \omega_\nu(\mathbf{k}'-\mathbf{k}))}{e^{\beta\hbar\omega_\nu(\mathbf{k}'-\mathbf{k})} - 1} \right. \\ &\left. + \frac{\delta(\omega(\mathbf{k}') - \omega(\mathbf{k}) + \omega_\nu(\mathbf{k}'-\mathbf{k}))}{1 - e^{-\beta\hbar\omega_\nu(\mathbf{k}'-\mathbf{k})}} \right\}, \end{aligned} \tag{15}$$

where $S = \sqrt{3}a^2/2$ is the area of a 2D graphite unit cell, d_t is the nanotube diameter, and the summation in Eq. (15) is over a series of points on cutting lines that satisfy both energy and momentum conservation. From Eq. (15), we can obtain the relaxation time for each phonon mode as well as the total relaxation time.[12]

We fit the carbon $2p_z$ orbital and the carbon atomic potential by a set of Gaussians to calculate $\mathbf{m}_\sigma$ in Eq. (11). The resulting integrals can be evaluated analytically.[23] The de-

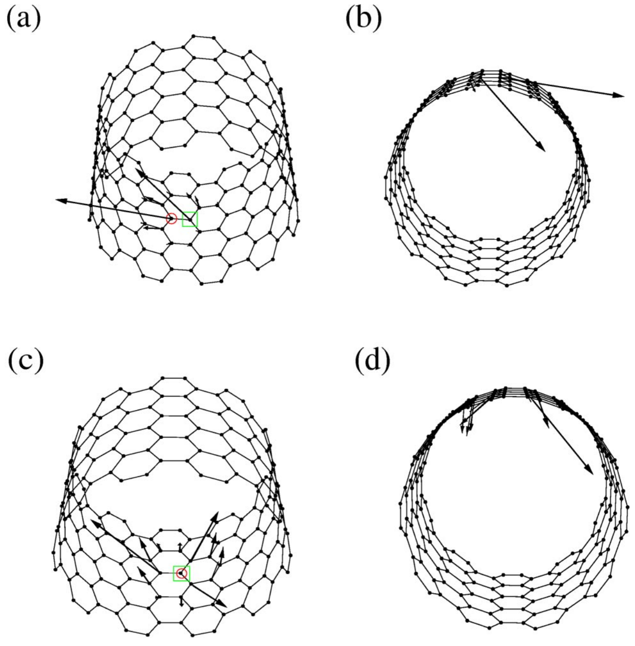

FIG. 5. The atomic deformation potential vectors defined by Eq. (11) as a function of the wave-function position of $\phi(\mathbf{r}-\mathbf{R}_{s'})$ for a (10,10) nanotube. The origins of $\boldsymbol{\nabla}v(\mathbf{r}-r_\sigma)$ and $\phi(\mathbf{r}-\mathbf{R}_s)$ are fixed for each figure and are denoted by an open square and circle in (a) and (c). (a) and (b) [side view of (a)] are the case having the largest value of the atomic deformation potential vector, while (c) and (d) [side view of (c)] are the case having the second largest value of the atomic deformation potential vector.

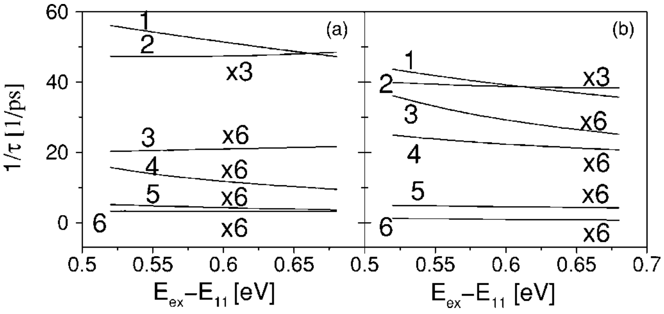

FIG. 6. The electron relaxation rate dependence on the initial electron state energy for a (6,5) nanotube; (a) and (b) correspond to ABAV and ABEV processes, respectively. In (a), the lines labeled from 1 to 6 are for the RBM, TW, oTO, LO, LA, and TO phonon modes, respectively. In (b), the lines labeled from 1 to 6 are, respectively, for the oTA, iTA, oTO, TO, LA, and LO zone-boundary modes. LA, iTA, TW, RBM, oTA, oTO, LO, and TO represent longitudinal acoustic, in-plane transverse acoustic, twisting, radial breathing, out-of-plane transverse acoustic, out-of-plane transverse optical, longitudinal optical, and transverse optical modes, respectively.

tailed evaluation will be given elsewhere. In graphite, the carbon $2p_z$ orbitals are parallel to each other along the out-of-plane direction, and thus $\mathbf{m}_\sigma$ has no out-of-plane components. It then follows that the out-of-plane phonon modes have no *e*-ph coupling in graphite.[12] In SWNTs, on the other hand, the $2p_z$ orbitals are perpendicular to the nanotube sidewall. Due to the curvature effect in SWNTs, $\mathbf{m}_\sigma$ has a component perpendicular to the nanotube surface ($m_{\sigma,\perp}$), which contributes to the *e*-ph coupling for the RBM and oTO modes. In Fig. 5, we show the deformation potential vectors for a (10,10) nanotube. Equation (11) indicates that the deformation potential vector $\mathbf{m}_\sigma$ is a three center integral, i.e., with a potential center and two electron centers. Figures 5(a) and 5(b) show the deformation potential vectors with an electron center on a nearest-neighbor site of the potential center and Figs. 5(c) and 5(d) are for the case with one electron and the potential having the same center. The deformation potential vector $|\mathbf{m}_\sigma|$ has a maximum value (≈ 6.4 eV/Å) when two electron centers are at the same site and the potential center is on a nearest-neighbor site and for this case, $m_{\sigma,\perp}\approx 0$ [see Figs. 5(a) and 5(b)]. When one electron has the same center as the potential and another electron center is on a nearest-neighbor site, we have two possible cases [see Figs. 5(c) and 5(d)]. One case is that the bond connecting the two electron centers is along the circumferencial direction. For this case, $|\mathbf{m}_\sigma|$ has a second maximum value (≈ 5.1 eV/Å). The other case is that the bond is not along the circumferencial direction. For this case, $|\mathbf{m}_\sigma|$ (≈ 3.3 eV/Å) has a third maximum value. For both of these two cases, $\mathbf{m}_\sigma$ has a nonvanishing $m_{\sigma,\perp}$ component. It is noted that a vector with a second maximum value of $|\mathbf{m}_\sigma|$ can also be seen in Figs. 5(a) and 5(b).

B. Relaxation time and Raman intensity calculation

As discussed in Sec. II, the phonon modes in SWNTs can be labeled by a cutting line index μ and a 1D wave vector q. However, it is not easy to get an intuitive picture for a phonon mode labeled by (μ,q). In the lower phonon frequency region, SWNTs have some special phonon modes, which do not have corresponding phonon modes in graphite, and we have special names for these modes.[3] In the higher phonon frequency region, although the phonon modes in SWNTs and graphite also have different properties, we can find corresponding phonon modes in graphite for the modes in SWNTs.[3] Thus we can use the names for the special nanotube modes and the names for graphite modes together to label all phonon modes in SWNTs. Hereafter, we will use this method to label phonon modes.

We calculate the relaxation time associated with each mode by using Eq. (15). The calculated results for each mode for a (6,5) nanotube are shown in Fig. 6. The initial electron state energy in Fig. 6 is smaller that E_{22} and thus the results are for AB transitions with electrons in the conduction subband for E_{11}. It is seen that when the initial electron energy is far from E_{11}, the relaxation rate is not sensitive to the excitation energy. Furthermore, for the AV process, the relaxation rate is dominated by the RBM. The relaxation time for the RBM is about 0.017 ps, which is about 24 times smaller than that for the LO mode. The TW mode also relaxes fast and the relaxation time for the TW mode is about 0.067 ps. For the EV transition, the relaxation rate is dominated by the oTA zone-boundary mode. The relaxation time for the oTA mode is about 0.025 ps. The iTA zone-boundary mode also relaxes fast, i.e, its relaxation time is about 0.077 ps. Summing over all these processes, the electron relaxation time of the (6,5) nanotube is on the order of 0.01 ps, which corresponds to the experimental observation that optically excited electrons in SWNTs can relax to E_{11} within about 0.1 ps.[6,24–26]

If the initial and final electron states are identical, $D^\nu(\mathbf{k},\mathbf{k})$ corresponds to the matrix for the first-order resonance Raman process and only $q=0$ phonon modes contribute to the e-ph coupling. For this case, $D^\nu(\mathbf{k},\mathbf{k})$ can be written as

$$D_\nu(\mathbf{k},\mathbf{k}) = \sum_{s,s'=A,B}\sum_{\mathbf{R}_{s'},\mathbf{R}_s}^{N_u} C_{s'}^*(\mathbf{k})C_s(\mathbf{k}) \times e^{-i\mathbf{k}\cdot(\mathbf{R}_{s'}-\mathbf{R}_s)}\mathbf{e}_A^\nu \times [\mathbf{m}_A(\mathbf{R}_{s'},\mathbf{R}_s) \pm U(\phi_{BA})\mathbf{m}_B(\mathbf{R}_{s'},\mathbf{R}_s)], \qquad (16)$$

where ϕ_{BA} is the rotation angle from a B atom to an A atom in a graphite unit cell around the z axis, and $+$ is for both the acoustic modes and for the RBM, while $-$ is for optical modes. From Eq. (16), we can get some interesting results. Due to the inversion symmetry of graphite, for an atom pair $(\mathbf{R}_{s'},\mathbf{R}_s)$ we can find a corresponding atom pair $(\mathbf{R}'_{s'},\mathbf{R}'_s)$, for which the phase factor in Eq. (16) is the same and $m_{A,\perp}(\mathbf{R}_s,\mathbf{R}_s)=Um_{B,\perp}(\mathbf{R}'_{s'},\mathbf{R}'_s)$, while $m_{A,\parallel}(\mathbf{R}_{s'},\mathbf{R}_s) =-Um_{B,\parallel}(\mathbf{R}'_{s'},\mathbf{R}_s)$ and $m_{A,z}(\mathbf{R}_{s'},\mathbf{R}_s)=-Um_{B,z}(\mathbf{R}'_{s'},\mathbf{R}'_s)$. Where $m_{\sigma,\parallel}$ is the component of $\mathbf{m}_\sigma$ along the circumferencial direction. It follows that the LA, TW, and oTO modes have no e-ph coupling for the $q=0$ case, which explains the experimental results, that we can only observe the RBM and G-band Raman spectra for first-order processes. For zigzag tubes, we find that $D=0$ for the TO mode, indicating that the TO mode is not a Raman-active mode. For armchair tubes, $D\neq 0$ for the LO mode. However, for a wave vector $\mathbf{k}$ in an armchair tube, we can find a corresponding wave vector $\mathbf{k}'$, which has the same energy as $\mathbf{k}$ and is obtained from $\mathbf{k}$ by mirror reflection with respect to the KMK' line in the 2D BZ of graphite. We find that the matrix element D for the LO mode is opposite for these two wave vectors $\mathbf{k}$ and $\mathbf{k}'$, leading to a vanishing of the Raman intensity for the LO mode. Thus, the LO mode is also not a Raman-active mode for armchair tubes.

The above discussion can explain the dependence of the Raman experimental data on chiral angle.[27] These results also reproduce the predictions of group theory. The LO mode (at $q=0$) for armchair nanotubes and the TO mode (at $q=0$) for zigzag nanotubes are A_u modes. According to group theory they are therefore not Raman-active modes.[3] In Fig. 7, we show the Raman intensity dependence on laser energy for a (6,5) nanotube. In the calculation, we have used the calculated relaxation time for each mode for the parameter γ in the denominator of the formula for the Raman intensity.[28] The peaks in the figure come from two resonance processes with E_{11}; namely, the incident resonance Raman process and the scattered resonance Raman process. The broader peaks for the RBM come from the smaller lifetime of this mode. The figure also shows that the LO mode has a stronger intensity than the TO mode. As we have mentioned, achiral nanotubes have strict selection rules about vanishing of the Raman intensity because of the existence of inversion symmetry. For (6,5) tubes, which are not achiral tubes, the strict selection rules need to be relaxed because of the lack of inversion symmetry. Thus, for such tubes, the IR-active TO mode is expected to have weak Raman intensity, which agrees with experiment.

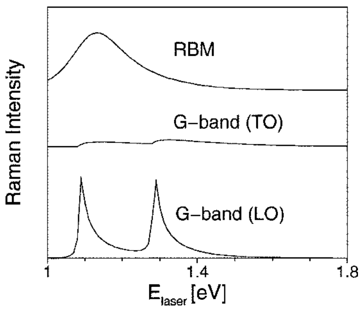

FIG. 7. RBM and G-band Raman intensity dependence on laser energy for a (6,5) SWNT. The calculated E_{11} value for the SWNT is about 1.1 eV.

IV. DISCUSSION

When we compare the relaxation time of SWNTs with that of graphite, we find that the relaxation time for SWNTs is at least one order of magnitude smaller than that for graphite. When graphite is rolled up to form carbon nanotubes, only the longitudinal phonon modes experience little change. From Fig. 6 we can see that the relaxation time for longitudinal modes is 0.1–1.0 ps, which corresponds to the result for graphite.[29] The tangential modes of a SWNT experience a big change due to curvature effects, e.g., the iTA mode turns into the TW mode. In particular, out-of-plane modes turn into RBM and oTO modes. As we have pointed out, graphite out-of-plane modes have no e-ph coupling. However, in SWNTs, the atomic deformation potential vectors can have a $m_{\sigma,\perp}$ component and thus the RBM and the oTO modes do have e-ph coupling, especially for small diameter nanotubes. From our calculations, we find that the e-ph coupling for the RBM and the oTO modes can be strong even in nanotubes with typical diameters. For example, for the (10,10) nanotube, the e-ph coupling strength for the RBM and oTO mode are, respectively, about 5 and 2 times larger than for the longitudinal modes. In addition, compared with graphite, the relaxation rate for the TW mode is also enhanced by curvature. In SWNTs the dominant contribution to the relaxation rate comes from the RBM, TW, and oTO modes, which cause SWNTs to have a much shorter relaxation time compared with graphite. Therefore the curvature effect enhances the e-ph coupling and decreases the inelastic mean free path in SWNTs compared with graphite.

In Fig. 6 we have shown the electron relaxation rate by phonon scattering in an energy region far from E_{11}. We find that the relaxation rate in this figure is not sensitive to the excitation energy. However, when the initial electron energy is close to E_{11}, the behavior of the relaxation rate dependence on the excitation energy is completely different. The results are shown in Fig. 8, where a series of peaks are seen. The shape of the peaks in Fig. 8 is similar to the peaks in the DOS or in the JDOS in SWNTs.[3,9] The mechanism of the spikes here is different from those in the DOS and JDOS

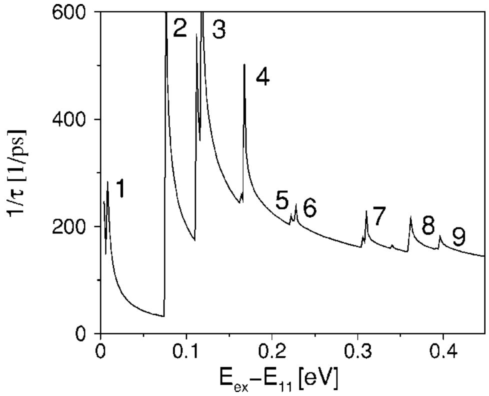

FIG. 8. The singularities in the relaxation rate near E_{11} for a (6,5) SWNT. The peaks labeled from 1 to 9 correspond to the acoustic, RBM, oTA (near K), oTO (near K), oTO, iTA (near K), iLA (near K), TO, and LO phonons, respectively.

spectra because here there is only one vHS point (E_{11}). The excited electron relaxes by emitting or absorbing a phonon. By absorbing a phonon, the electron gains energy and jumps to a higher energy state. By emitting a phonon, the electron loses energy and jumps to a lower energy state. Obviously, by absorbing or emitting a phonon, the electron energy will move away from or closer to E_{11}. If the excited electron can jump to E_{11} by emitting only one phonon, the relaxation rate will be dramatically increased, due to the van Hove singularity in the density of states at E_{11}.

In this case, a high intensity peak appears in Fig. 8 and the absorption rate can be neglected. The position of the peak reflects the phonon energy for a special phonon mode. The height and width of the peak reflect the e-ph interaction strength. In the Fig. 8 we identify the corresponding phonon modes for each peak. This interesting finding has important implications for PL experiments. By absorbing laser energy, electrons in the valence band are excited to the conduction band. By emitting a phonon, the excited electrons go down in energy, moving towards the conduction band extremum and the holes go up in energy towards the valence band extremum by emitting phonons. In the course of the processes by which electrons and holes go toward E_{11}, some electrons will combine with holes *before* their energy separation becomes E_{11} due to hot electron emission. After the electrons and holes arrive at their respective band extrema, electrons will combine with holes by emitting light at energy E_{11}. The intensity of the emitted light depends on how many electrons have been lost along the way to E_{11}.

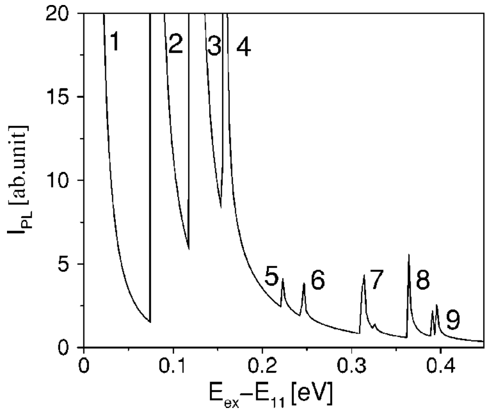

FIG. 9. The PL intensity by the *one-phonon emission* process. The peaks labeled from 1 to 9 correspond to the same phonon modes as are labeled in Fig. 8.

If the electrons can arrive at E_{11} by emitting only one phonon, a bright spot will appear in the PLE plots. This *two-phonon emission* process is illustrated in Fig. 2(b). The condition for this process is $E_{\rm ex}=E_{11}+2\hbar\omega$. The factor 2 comes from the fact that both the electron and hole should emit phonons with the same energy. To calculate the intensity for this kind of *one-phonon emission* PL, we introduce the formula

$$I_{\rm PL}=I_a(E_{\rm ex})\frac{1}{\tau}I_e(E_{\rm ex}-2\hbar\omega), \tag{17}$$

where $I_a(E_{\rm ex})$ and $I_e(E_{\rm ex}-2\hbar\omega)$ are the optical absorption and emission intensities at the initial and final states. The calculated PL intensity is shown in Fig. 9 as a function of $E_{\rm ex}-E_{11}$. A series of peaks can be clearly seen. The peaks with large intensity are located at $E_{\rm ex}=E_{11}$, $E_{11}+2\hbar\omega_{\rm RBM}$, $E_{11}+2\hbar\omega_{\rm G}$. The theoretical results correspond well with recent experimental data.[17] Each peak in the figure has a corresponding experimental peak and the relative intensities of the peaks in Fig. 9 also agree well with the experimental data.

From Fig. 2, we know that in the PL process an electron can emit phonons not only by a transition between two real states but also by a transition mediated by a virtual state, in a so-called Raman process. In Fig. 3 we illustrate how the PL by the Raman process can be observed in a schematic PLE plot. In the experimental PLE plot, we expect to see several bright spots on a vertical line at $E_{\rm PL}=E_{11}$, and we can also see several lines making an approximately 45° angle with the $E_{\rm ex}$ axis. These lines are due to resonance Raman processes observed in the PL spectra. In the Raman process, we have $E_{\rm ex}=E_{\rm laser}$ and $E_{\rm PL}=E_{\rm laser}-\hbar\omega$. Thus we get a simple relationship between $E_{\rm ex}$ and $E_{\rm PL}$, i.e., $E_{\rm ex}=E_{\rm PL}+\hbar\omega$. From this equation, we know that the line due to the Raman process makes a 45° angle with the $E_{\rm PL}$ axis. Moreover, from the measured $E_{\rm ex}$ and $E_{\rm PL}$ values for a point on this line, we can get the phonon energy.

In Fig. 10 we show the calculated PL intensity dependence on $E_{\rm ex}$ and $E_{\rm PL}$ for the (6,5) nanotube in which the intensity is expressed by the thickness of the line. There are

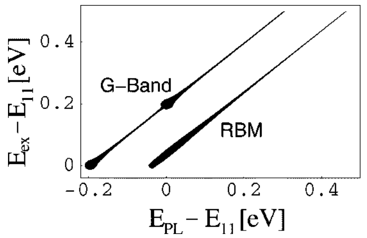

FIG. 10. PL due to Raman processes. The thickness of the lines represents the PL intensity. The results for the RBM and G-band (LO mode) are labeled.

two lines in the figure, which come from the RBM and G-band phonons. For the (6,5) nanotube, the LO mode is predicted to have a much stronger Raman intensity than the TO mode. Thus the G-band line in the figure mainly comes from the LO mode. Around $E_{\mathrm{PL}}=E_{11}$ and $E_{11}-0.2$ eV the G-band feature has a large intensity. This is due to two resonance conditions with E_{11}: $E_{\mathrm{laser}}=E_{11}$ (the incident resonance Raman process) and $E_{\mathrm{laser}}=E_{11}+\hbar\omega$ (the scattered Raman process). The RBM phonon energy is about 0.035 eV, which is relatively small compared to that for the other phonons, and thus there is a large PL intensity around $E_{\mathrm{PL}}=E_{11}$ in Fig. 10. Both the G-band line and RBM line are found in the experimental data.[17] Furthermore, we can clearly see two large intensity regions for the G-band line in the experimental PL plots. Some lines with an approximately 45° angle cannot be explained by a first-order Raman process because for these lines $E_{\mathrm{ex}}>E_{\mathrm{PL}}+0.2$ eV. These lines are due to second-order resonance Raman processes (as for example, for the G' band), which are not discussed here.

V. SUMMARY

In summary, we have carried out calculations to explain electron relaxation processes in PLE experiments. Two important relaxation processes, i.e., the *two-phonon emission* process and the Raman process, are pointed out theoretically. Because of the cylindrical shape of a SWNT, the deformation potential has a coupling with out-of-plane phonon modes, such as the RBM and oTO phonon modes in SWNTs. The relaxation time calculation shows that the RBM and TW phonon modes give a dominant contribution to the relaxation rate among the various intravalley phonon mode processes, while the oTA and iTA make a large contribution for the intervalley phonon mode processes. The PL intensity for these two processes are calculated and reproduce the experimental PLE plot very well.[17] The Raman intensity is strongly enhanced when the scattering resonance conditions are obeyed.

ACKNOWLEDGMENTS

R.S. acknowledges a Grant-in-Aid (No. 13440091) from the Ministry of Education, Japan. MIT authors acknowledge support under NSF Grants DMR 04-05538 and INT 00-00408, and the Dupont-MIT alliance. A.J. acknowledges financial support from CNPq and FAPEMIG, Brazil, and from JST–Japan for supporting his visit to Tohoku University.

[1] M. J. O'Connell, S. M. Bachilo, X. B. Huffman, V. C. Moore, M. S. Strano, E. H. Haroz, K. L. Rialon, P. J. Boul, W. H. Noon, C. Kittrell, J. Ma, R. H. Hauge, R. B. Weisman, and R. E. Smalley, Science **297**, 593 (2002).

[2] A. Hartschuh, H. N. Pedrosa, L. Novotny, and T. D. Krauss, Science **301**, 1354 (2003).

[3] R. Saito, G. Dresselhaus, and M. S. Dresselhaus, *Physical Properties of Carbon Nanotubes* (Imperial College Press, London, 1998).

[4] S. M. Bachilo, M. S. Strano, C. Kittrell, R. H. Hauge, R. E. Smalley, and R. B. Weisman, Science **298**, 2361 (2002).

[5] T. Hertel and G. Moos, Phys. Rev. Lett. **84**, 5002 (2000).

[6] O. J. Korovyanko, C.-X. Sheng, Z. V. Vardeny, A. B. Dalton, and R. H. Baughman, Phys. Rev. Lett. **92**, 017403 (2004).

[7] T. Hertel and G. Moos, Chem. Phys. Lett. **320**, 359 (2000).

[8] G. Moos, R. Fasel, and T. Hertel, J. Nanosci. Nanotechnol. **3**, 145 (2003).

[9] Ge. G. Samsonidze, R. Saito, A. Jorio, M. A. Pimenta, A. G. Souza Filho, A. Grüneis, G. Dresselhaus, and M. S. Dresselhaus, J. Nanosci. Nanotechnol. **3**, 431 (2003).

[10] R. Saito, A. Jorio, A. G. Souza Filho, G. Dresselhaus, M. S. Dresselhaus, and M. A. Pimenta, Phys. Rev. Lett. **88**, 027401 (2002).

[11] C. F. Klingshirn, *Semiconductor Optics* (Springer, Berlin, 2004).

[12] J. Jiang, R. Saito, A. Grüneis, G. Dresselhaus, and M. S. Dresselhaus, Chem. Phys. Lett. **392**, 383 (2004).

[13] J. Lefebvre, Y. Homma, and P. Finnie, Phys. Rev. Lett. **90**, 217401 (2003).

[14] Ge. G. Samsonidze, R. Saito, N. Kobayashi, A. Grüneis, J. Jiang, A. Jorio, S. G. Chou, G. Dresselhaus, and M. S. Dresselhaus, Appl. Phys. Lett. **85**, 5703 (2004).

[15] S. M. Bachilo, L. Balzano, J. E. Herrera, F. Pompeo, D. E. Resasco, and R. B. Weisman, J. Am. Chem. Soc. **125**, 11186 (2003).

[16] S. G. Chou, H. B. Ribeiro, E. Barros, A. P. Santos, D. Nazich, Ge. G. Samsonidze, C. Fantini, M. A. Pimenta, A. Jorio, F. Plentz Filho, M. S. Dresselhaus, G. Dresselhaus, R. Saito, M. Zheng, G. B. Onoa, E. D. Semke, A. K. Swan, M. S. Ünlü, and B. B. Goldberg, Chem. Phys. Lett. **397**, 296 (2004).

[17] S. G. Chou *et al.* (unpublished).

[18] J. Jiang, R. Saito, A. Grüneis, G. Dresselhasu, and M. S. Dresselhasu, Carbon (to be published).

[19] R. Saito, G. Dresselhaus, and M. S. Dresselhaus, J. Appl. Phys. **73**, 494 (1993).

[20] R. Saito, R. Matsuo, T. Kimura, G. Dresselhaus, and M. S. Dresselhaus, Chem. Phys. Lett. **348**, 187 (2001).

[21] H. Suzuura and T. Ando, Phys. Rev. B **65**, 235412 (2002).

[22] C. L. Kane and E. J. Mele, Phys. Rev. Lett. **78**, 1932 (1997).

[23] A. Grüneis, Ph.D. thesis, Tohoku University (2004).

[24] J. S. Lauret, C. Voisin, G. Cassabois, C. Delalande, Ph. Roussignol, O. Jost, and L. Capes, Phys. Rev. Lett. **90**, 057404 (2003).

[25] Y.-Z. Ma, J. Stenger, J. Zimmermann, S. M. Bachilo, R. E. Smalley, R. B. Weisman, and G. R. Fleming, J. Chem. Phys. **120**, 3368 (2004).

[26] H. Hippler, A.-N. Unterreiner, J.-P. Yang, S. Lebedkin, and M. M. Kappes, Phys. Chem. Chem. Phys. **6**, 2387 (2004).

[27] Z. Yu and L. E. Brus, J. Phys. Chem. B **105**, 1123 (2001).

[28] C. Thomsen and S. Reich, Phys. Rev. Lett. **85**, 5214 (2000).

[29] K. Seibert, G. C. Cho, W. Kütt, H. Kurz, D. H. Reitze, J. I. Dadap, H. Ahn, M. C. Downer, and A. M. Malvezzi, Phys. Rev. B **42**, 2842 (1990).